Integrated Circularly Polarized OAM Generator and Multiplexer for Fiber Transmission

Yuxuan Chen, Leslie A. Rusch, and Wei Shi

IEEE Journal of Quantum Electronics, (Volume 54, Issue 2) (2017)

Doi: 10.1109/JQE.2017.2780448

https://ieeexplore.ieee.org/abstract/document/8168404/

Integrated Circularly Polarized OAM Generator and Multiplexer for Fiber Transmission

Yuxuan Chen, Leslie A. Rusch, *Fellow, IEEE*, and Wei Shi, *Member, IEEE*

***Abstract*—Unlike linearly polarized modes in fiber, modes exploiting orbital angular momentum (OAM) are circularly polarized when propagating in fiber. The use of OAM modes for spatial multiplexing requires efficient, low cost mode generators and multiplexers. We propose such a device based on the standard 220-nm silicon-on-insulator platform, taking multiple single-mode data-modulated signals, and imprinting these signals on right- and left-circularly polarized OAM channels on a single, multiplexed output. The device is designed to easily couple to an OAM fiber with a ring shaped core. This approach treating circular polarization within the multiplexer allows us to avoid the losses associated with filtering out unwanted polarization to create a single polarization. Designing the device to have an output matched to the OAM fiber mode profile also avoids mode size conversion. We describe our design methodology and optimization techniques using a transfer-matrix model and the finite-difference time-domain method. A candidate design is simulated and modal crosstalk is examined, showing that low-crosstalk OAM multiplexing can be achieved through direct fiber-to-chip coupling.**

***Index Terms*—Silicon photonics, circular polarization, orbital angular momentum, space division multiplexing, fiber-to-chip coupling, WDM compatible, integrated photonic circuits.**

I. Introduction

SPACE division multiplexing (SDM) in optical fiber can increase transmission capacity while reducing the cost per bit; it can be combined with quadrature modulation and multiplexing in time, frequency, and polarization. SDM can be applied to multicore and few mode fibers, or hybrids where each core carries a few modes [1]. Most few mode fiber (FMF) SDM systems exploit linearly polarized (LP) modes as they are well-studied and easy-to-generate. LP modes are linear combinations of fiber eigenmodes; LP modes with eigenmodes in common see significant crosstalk, hence these SDM systems commonly employ multi-input multi-output (MIMO) processing at the receiver [2][3]. Scaling such SDM systems to higher numbers of modes requires large monolithic receivers and complex MIMO processing. Orbital angular momentum (OAM) modes are an alternate modal basis for SDM [4]. Unlike LP modes, OAM modes are formed from only two eigenmodes, with the same propagation constant, and among OAM modes there are no shared (i.e., no common) eigenmodes. The coupling between OAM modes is low, at least for short distances (data center or local access). With low crosstalk, MIMO processing could be greatly reduced, a monolithic receiver is not required, and system complexity and power consumption could be reduced.

The authors are with the Department of Electrical and Computer Engineering, Centre for Optics, Photonics and Lasers (COPL), University of Laval, Quebec, QC G1V 0A6, Canada (e-mail: yuxuan.chen.1@ulaval.ca; leslie.rusch@gel.ulaval.ca; wei.shi@gel.ulaval.ca).

The OAM mode phasor is $exp(jl\Phi)$, where l is the topological charge; the sign of the topological charge indicates the direction of phase evolution [5]. In the laboratory, OAM modes can be easily generated in free space using spatial light modulators (SLM) [6][7][8]. Fundamental, Gaussian shaped light is projected on an SLM programmed to generate the desired OAM topological charge. Free-space OAM multiplexers combine data-modulated OAM modes through lenses before coupling into OAM fibers. Such free-space OAM setups are very bulky, cumbersome, and vulnerable to even tiny changes in alignment. These challenges are quickly magnified as the number of OAM modes increases.

The silicon on insulator (SOI) platform offers robustness, compactness and tunability; it has produced OAM generators and multiplexers. Ultra-compact OAM generaters can be implemented using micro-ring resonators [9], which, however, are not WDM-compatible since the OAM order depends on the resonant wavelength. In [10], the optical signal passes through a series of concentric 1D grating couplers, leading to a beam amplitude mimicking that of an OAM beam. Next a bus waveguide assigns the proper phase characteristics for OAM generation. In [11], the phase assignment is accomplished by a star coupler instead of a bus waveguide, and a 3D waveguide is used to convert the phase and amplitude distribution at the output. OAM modes are generated in free space in these devices, and encounter two challenges when coupling the output into an OAM fiber. Firstly, the beams generated by these devices have azimuthal or radial polarization, while fiber OAM modes must be circularly polarized. As a result, these OAM generators cannot directly create (left and right) polarization multiplexed signals. Two devices would be required and their outputs filtered (to isolate one circular polarization) and then two outputs combined. In either case, single polarization or polarization multiplexed, there is an associated 3 dB loss in output power. Secondly, the mode sizes of the previous SOI device are at least one magnitude higher than fiber OAM modes; lens are required to shrink mode sizes, resulting in extra loss and higher system complexity.

In this paper, we present the design and optimization methodology of a SOI based circular-polarized OAM generator and multiplexer targeting direct fiber coupling. The sizes of the generated OAM modes are designed to match the waveguide in ring core OAM fiber [12]; only minimal free-space optics are needed for OAM fiber coupling. In Section II, our design principle and simulation model are introduced. Simulation results are presented and discussed in Section III. Concluding remarks are made in Section IV.

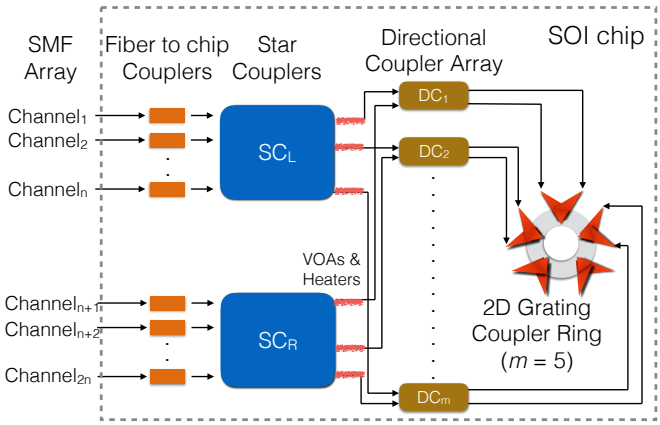

Fig. 1: Schematic of the SOI OAM generator and multiplexer; in this example the number of 2D grating couplers is m=5.

II. Principle and Model

A. Principle of Operation

A block diagram of our OAM generator and multiplexer is shown in Fig. 1. It serves as the bridge between multiple SMF inputs carrying modulated data, and the single, ring-core OAM fiber to carry the spatially multiplexed signals. The SOI-based, integrated circuit encodes each input SMF onto a distinct OAM mode and polarization supported by the OAM fiber. The input channels (far left, Fig. 1) map to unique OAM states, distinguished by their polarization, topological charge and direction of rotation of the phase front. The topological charge is an integer, the direction of rotation is the sign of the topological charge.

As seen in Fig. 1, the inputs are separated into two sections based on the handedness of the intended polarization state at the output. The star coupler marked SC_L transforms signals destined for left circular polarization, while star coupler SC_R handles signals for right circular polarization. Each star coupler performs the same task of transforming the topological charge and rotating the phase front of its inputs appropriately. After that, light from the star couplers is sent to different ports of a directional coupler array to achieve the appropriate polarization. Finally, the 2D grating couplers (2D-GCs) are properly designed and placed so that the dimensions of the output OAM modes match with the mode sizes in ring-core OAM fiber [12]. The chip function and operation is entirely symmetrical from input to output. It could be used as a demultiplexer as well by reversing the propagation direction of the light. In the following, our analysis focuses on the multiplexer function. We use the transfer matrix method to find the electric fields as light propagates through the device. We assume fundamental TE mode operation in all the on-chip waveguides in our simulations.

B. Transfer Matrix Model

The fiber-to-chip couplers in Fig. 1 are the optical inputs to the device. The transfer matrix for each section of the fiber-to-chip couplers is an identity matrix multiplied by η_c, where η_c is the coupling efficiency of the fiber-to-chip coupler. Each input is mapped to a unique OAM state. The number of fiber-to-chip couplers should match the maximum number of OAM states supported by the target OAM fiber. We let n be the number of input channels for each polarization state.

The two star couplers in Fig. 1 split light from the fiber-to-chip couplers, and imprint each input with the proper phase for OAM generation. The upper star coupler is dedicated to left circular polarization (LCP), the lower one to right circular polarization (RCP). As mentioned earlier, the star couplers are named for the intended polarization states, but the star couplers themselves only manage the phase **not** polarization. In wavelength division multiplexing applications, star couplers are used in pairs to separate different wavelength channels [13]. In our case, we instead exploit the free propagation region of the star coupler to create the phase differences needed for OAM.

Star coupler input and output ports are arranged in a Rowland circle geometry targeting even splitting of light. As light from the input ports diverges within the free propagation region, the output port amplitudes tend to vary. This can be balanced through on-chip variable optical attenuators (VOAs). The influence of this amplitude non-uniformity on crosstalk performance is discussed in section B of the appendix. For the analysis in the main body of the paper we assume uniform amplitude.

Assuming no loss, the amplitude at each output would be $1/\sqrt{m}$ when there are m outputs. As for the phase, by carefully designing the position of the input and output ports as well as the length of the free propagation region, the phase difference between adjacent output ports (due to differences in the optical path) would be a multiple of $2\pi/m$. Thus, the transfer matrix for the star coupler, M_{SC}, would be a $m \times n$ matrix, where m is the number of 2D-GCs used in the grating coupler ring. We have

$$M_{SC} = \begin{bmatrix} s_{1,1} & \cdots & s_{1,n} \\ \vdots & s_{p,q} & \vdots \\ s_{m,1} & \cdots & s_{m,n} \end{bmatrix} \tag{1}$$

in which

$$s_{p,q} = \frac{e^{i\varphi_{p,q}}}{\sqrt{m}} \tag{2}$$

where $\varphi_{p,q}$ represents the phase assigned to the p^{th} output port from the q^{th} input port. Supposing that the intended OAM topological charge at q^{th} input port is l, and the intended polarization is LCP, we have

$$\varphi_{p,q} = \frac{2\pi(l+1)(p-1)}{m} \tag{3}$$

and if the intended polarization is RCP, then

$$\varphi_{p,q} = \frac{2\pi(l-1)(p-1)}{m} \tag{4}$$

The outputs of SC_L are routed to the upper ports of each directional coupler in the directional coupler array while the outputs of SC_R are routed to the lower ports. Intersecting (or crossing) waveguides are inevitable in this architecture, as illustrated in Fig. 1. The waveguide crossing on the SOI

platform has demonstrated loss below 0.03 dB, and crosstalk below -37 dB at both O-band and C-band [14]. Thus, it is reasonable to neglect the effect of waveguide crossing in the current model. However, as we scale up the number of output ports, this assumption may no longer hold; these effects may well be included in our future simulations.

The directional coupler consists of two parallel waveguides. It is commonly used in splitting or combining light in photonic circuits. A design with a 50-50 splitting ratio is assumed, where light passing through the directional coupler via the upper port is evenly split between the two output ports, with a 90 degree phase shift. Light entering via the lower input port will also be evenly split, but with a negative 90 degree phase shift. The net effect creates an integrated version of a quarter waveplate. The transfer matrix for a single directional coupler is as follows

$$M_{DC} = \frac{\sqrt{2}}{2}\begin{bmatrix} 1 & e^{i\frac{\pi}{2}} \\ e^{i\frac{\pi}{2}} & 1 \end{bmatrix}. \tag{5}$$

The 2D grating coupler ring is the optical output of this device, consisting of m individual 2D-GCs. The 2D-GCs are attractive for on-chip polarization diversity [15][16]. While most components on the SOI platform have TE orientation, 2D-GC are designed to deal with polarization uncertainty. For instance, they can be used to couple light with arbitrary polarization following fiber transmission. The 2D-GC can be viewed as two identical 1D grating couplers whose grating regions overlap at a 90 degree angle. Light with arbitrary linear polarization is thereby split into two orthogonal linear polarizations. Manipulating the amplitudes and phases of the two linearly polarized components, any linear polarization can be obtained. In our case, combining the two linearly polarized components as inputs to the 2D-GC with equal amplitude, a positive 90 degree phase shift generates LCP emission, while a negative phase shift gives RCP. The transfer matrix of a single 2D-GC is 1×2, since the light from two input arms is combined after emission. For the p^{th} 2D-GC in the grating coupler ring, its contribution in polarization can be expressed as

$$M_{GC,p} = \begin{bmatrix} M_{arm1,p} & M_{arm2,p} \end{bmatrix} \tag{6}$$

in which

$$M_{arm1,p} = \begin{pmatrix} -\sin\theta_p \\ \cos\theta_p \end{pmatrix}; \quad M_{arm2,p} = \begin{pmatrix} -\cos\theta_p \\ -\sin\theta_p \end{pmatrix} \tag{7}$$

where $M_{armi,p}$ is the local linear polarization of arm i, and θ_p indicates the position of the 2D-GC in the ring and is given by

$$\theta_p = 2\pi(p-1)/m. \tag{8}$$

The total transfer matrix for all on-chip components is found by multiplying the transfer matrices in sequence

$$M_{on-chip} = \begin{bmatrix} t_{1,1} & \dots & t_{1,2n} \\ \vdots & t_{p,q} & \vdots \\ t_{m,1} & \dots & t_{m,2n} \end{bmatrix} \tag{9}$$

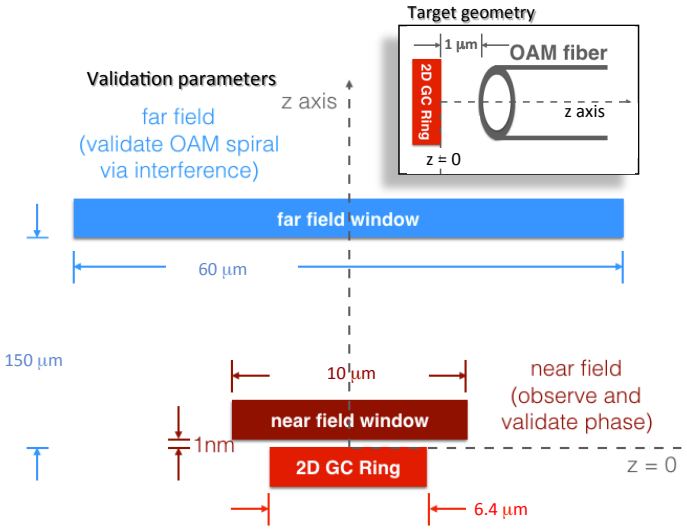

Fig. 2: Illustration of coupling scenario (inset) and free-space propagation simulation for near and far field.

if $q \le n$,

$$t_{p,q} = -\frac{1}{2}\eta_c i \begin{pmatrix} 1 \\ i \end{pmatrix} e^{-i\theta_p} \left(\frac{1}{\sqrt{m}}\right) e^{i\varphi_{p,q}} \tag{10}$$

if $n \le q \le 2n$, then

$$t_{p,q} = -\frac{1}{2}\eta_c \begin{pmatrix} 1 \\ -i \end{pmatrix} e^{i\theta_p} \left(\frac{1}{\sqrt{m}}\right) e^{i\varphi_{p,q}} \tag{11}$$

where left hand $\binom{1}{i}$ and right hand $\binom{1}{-i}$ circular polarization are the result of the directional couplers and 2D-GCs, $e^{-i\theta_p}$ and $e^{i\theta_p}$ come from the 2D-GC, and $e^{i\varphi_{p,q}}/\sqrt{m}$ reflects the influence of the star couplers on amplitude and phase.

C. Free-space Propagation at Output

We are designing a multiplexer to be used with ring core fibers supporting OAM modes. In the inset of Fig. 2 we illustrate a typical coupling scenario where ring core fiber, here with 3.6 μm outer radius, is at a target 1 μm from the ring of m 2D-GCs. We must examine the properties of our multiplexed signal as it leaves the chip and propagates short distances in free space towards the ring core fiber input. The efficiency of coupling will vary with the separation between chip and fiber; we wish to evaluate this variation. We therefore include free-space transmission in our model, examining the electrical field throughout a hemisphere beginning at the output plane of the 2D-GCs, as seen in Fig. 2. The near field simulations will allow us to validate the phase profile achieved, and to calculate coupling efficiency as a function of spacing. The far field is used to validate the generated beams are indeed OAM modes; that distance allows production of classic OAM interferometric intensity spirals. The boundary for near field and far field is $2D^2/\lambda$ [17], where D is the diameter of the antenna, so for Gaussian beam waist of $w_0 = 1.5$ μm, near field goes up to 11.6 μm.

We have two simulators: 1) MATLAB™ for results in the main body of this paper, and 2) a numerical finite-difference time-domain (FDTD) solver for results in section A of the

appendix. Transfer matrix calculations (described previously), and the free space propagation (described in this section) are executed in MATLAB™. The FDTD simulator is used to validate assumptions made in free-space simulations. In particular, we validate numerically the assumption of 2D-GC output waves with a Gaussian intensity distribution and circular polarization.

Light emitted from 1D-GC is always optimized to produce a Gaussian beam [18]. Thus in our 2D-GC, two overlapping Gaussian beams, each with its own polarization state, combine to form the output beam. As we are not aware of any demonstrations assuring the Gaussian nature of the combined beams, we validate this assumption for free-space propagation before proceeding with our MATLAB™ simulations. Section A of the appendix shows FDTD simulations of the free-space OAM beams. They closely resemble beams with a Gaussian distributed intensity, with less than 1.5 dB deviation at distances around 1 μm. Note that this deviation could be improved using techniques from [19] for the 2D-GC design. Specifically, imperfections due to evanescent field in the cladding could be reduced by introducing a linear chirp in the grating period and adding end reflectors at the back of the grating. Therefore our MATLAB™ simulations are most accurate when the strong evanescent field outside of the grating region is minimized.

We assume that light emitted by the 2D-GC propagates in the $+z$ direction. We define

$$z_R = \frac{\pi {w_0}^2}{\lambda}. \tag{12}$$

Proceeding with the Gaussian assumption for a single 2D-GC output with beam waist w_0, and letting $\tilde{z}$ be the axial distance from the beam waist in a local coordinate system for that 2D-GC, the beam axial distribution is

$$w(\tilde{z}) = w(0)\sqrt{1 + \left(\frac{\tilde{z}}{z_R}\right)^2}. \tag{13}$$

We define

$$R(\tilde{z}) = \tilde{z}\left[1 + \left(\frac{z_R}{\tilde{z}}\right)^2\right]. \tag{14}$$

The output of the field of a single 2D-GC (in phasor form) is

$$\mathbf{E}(r,\tilde{z}) = E_0 \hat{c}\frac{w_0}{w(\tilde{z})} e^{\frac{-r^2}{w(\tilde{z})^2}} e^{-i(k\tilde{z} + k\frac{r^2}{2R(\tilde{z})} - \psi(\tilde{z}))} \tag{15}$$

where E_0 is the electric field at the center of the 2D-GC, $\hat{c}$ represents the circular polarization state of the beam (either LCP or RCP), i is the imaginary unit, r is the radial distance from a $\tilde{z}$ axis centered at that particular 2D-GC [20].

The field at an arbitrary point in the output free-space hemisphere is the result of interference among all 2D-GCs fields or, in other words, the sum of the collection of Gaussian beams. The radius of the grating coupler ring is $R_c = 3.2$ μm, and its center is the origin of our coordinate system, with the z-axis pointing out from the 2D-GC ring. For a fixed z, due to the circular symmetry of our design, the constructive interference occurs in donut shapes with intensity maxima appearing at a radial distance related to the topological charge of the targeted OAM modes. For example, if the intended topological charge is 0, the fields at the centers of the Gaussian beams are in phase, meaning that the constructive interference occurs on the z-axis ($r = 0$) . As the intended topological charge increases, the strongest constructive interference shifts outward radially, thus transforming into a donut shape. Since all the electric fields at the Gaussian beam centers have phase $e^{i\varphi_{p,q}}$, the phase distribution on any z plane is helical.

III. Simulation and Analysis

Our design creates a helical wave front by adjusting the phase at each 2D-GC. Near field simulations validate phase profile and find coupling efficiency as a function of spacing. Far field simulations produce interferometric intensity profiles.

A. Validating OAM Generation

To validate OAM generation we examine the phase profile at near field. Due to the finite number of 2D-GCs, the phase profile is discrete in nature, while true OAM phase profiles are continuous. We therefore also examine the OAM beams asymptotically, that is, in the far field. Via simulation, we propagate for longer distances and examine the interference of a reference Gaussian beam with the discrete-phase output beam at far field; we observe the expected spiral intensity pattern of true OAM beams.

The geometry of our simulation is as given in Fig. 2, with a small observation window in near field, and a larger one in far field. The radius R_c in our simulations is 3.2 μm. A waist of w_0 =1.5 μm was used for each Gaussian beam. We examined a total of $m = 5$ 2D-GCs. Note that the dimensions studied are feasible for fabrication, that is, a ring of radius 3.2 μm can accommodate five beams of waist 1.5 μm.

In the first two rows of Fig. 3 we present simulation results in the near field. The intensity and phase were observed at a near field where $z = 1$ nm, over an observation window 10 μm $\times$ 10 μm. Results are for exciting one fiber input for LCP at a time with a continuous wave. Each column in Fig. 3 shows the corresponding profiles, intensity in row 1 and phase in row 2, with the heading of the column indicating which order OAM mode was excited for the associated fiber input. In the first row we see the five Gaussian intensity distributions arranged in a ring. In the second row we see a discretized phase profile: zero phase for order zero, a single 2π phase distribution for orders plus/minus one, and two sweeps of 2π for orders plus/minus two.

In the bottom two rows of Fig. 3 we present simulation results in the far field. At a distance of z =150 μm, we beat the 2D-GC ring output with a reference Gaussian beam, either right or left circularly polarized. We observe the interference pattern generated across a 60 μm $\times$ 60 μm window. A clear spiral for order one can be seen on the third row of Fig. 3. In that case the OAM modes and the reference Gaussian beam share the same polarization. Since order two is the theoretical limit for $m = 5$ 2D-GCs, the phase of the generated beam is nevertheless discrete, thus the arm of the spiral cannot be continuous; the spiral shape is clearly visible. In the fourth row, as polarization states are orthogonal (RCP vs. LCP), spirals do not appear, confirming our polarization state is correct.

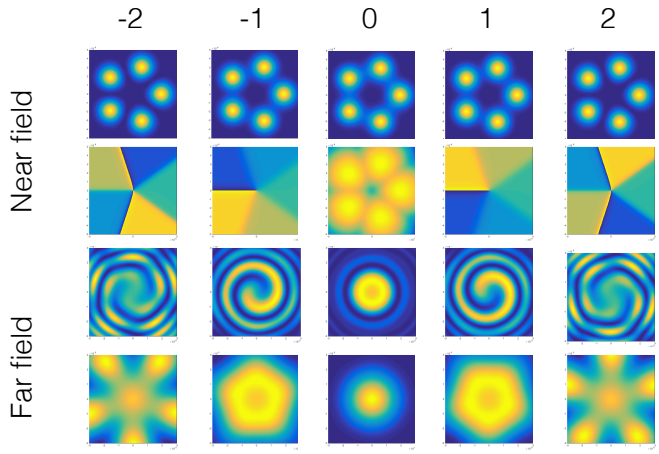

Fig. 3: OAM mode orders (all LCP) appear above columns; near field intensity shown in row one, phase in row two; far field interference patterns with reference LCP Gaussian beam in row three, with reference RCP Gaussian beam in row four.

B. Efficiency of Coupling into Fiber

In this section we fix the separation between the 2D-GC ring and the ring core fiber (RCF), and calculate the efficiency with which the targeted OAM mode is excited. We simulate a ring-core fiber supporting OAM modes to order two. This fiber was designed, fabricated and characterized as reported in [12]. We consider three multiplexer designs ($m = 5$, $m = 9$ and $m = 13$) to explore the impact of 2D-GC number on coupling efficiency. A companion analysis can be found in [21] that focuses on the purity of the excited OAM mode rather than the coupling efficiency.

The field profiles of the eigenmodes (EH and HE) supported by RCF4 in [12] can be found numerically from the fiber dimensions and refractive indices. The OAM fields are found from the eigenmodes per the following relationships [22]

$$\mathrm{OAM}^{\pm}_{\pm l,1} = \mathrm{HE}^{\mathrm{even}}_{l+1,1} \pm j\mathrm{HE}^{\mathrm{odd}}_{l+1,1} \tag{16}$$

$$\mathrm{OAM}^{\mp}_{\pm l,1} = \mathrm{EH}^{\mathrm{even}}_{l-1,1} \pm j\mathrm{EH}^{\mathrm{odd}}_{l-1,1} \tag{17}$$

where the OAM superscript indicates the polarization state (+ for RCP, - for LCP), the eigenmode superscript indicates its symmetry, the subscript l is the topological charge, or OAM order, and the second subscript is one as the OAM modes we target exhibit a single intensity ring.

We define the two dimensional integral of the fiber OAM mode electrical field, $\mathbf{E}_F$, to be

$$A_F = \iint \mathbf{E}^*_F \cdot \mathbf{E}_F dxdy \tag{18}$$

where * indicates complex conjugate.

Three parameters determine the electrical field of the OAM beam that exits the 2D-GC ring and propagates in free-space to the fiber input: R_c, w_0 and the free-space separation z_f between the fiber and the 2D-GC ring. We define the two dimensional integral of that electrical field, $\mathbf{E}_{GC}$, to be

$$A_{GC} = \iint \mathbf{E}^*_{GC} \cdot \mathbf{E}_{GC} dxdy \tag{19}$$

The coupling loss is given by the overlap integral at $z = z_f$ of the two electrical fields (fiber and free-space from 2D-GC), normalized appropriately, that is,

$$\frac{\iint \mathbf{E}^*_F \cdot \mathbf{E}_{GC} dxdy}{\sqrt{\iint \mathbf{E}^*_F \cdot \mathbf{E}_F dxdy \iint \mathbf{E}^*_{GC} \cdot \mathbf{E}_{GC} dxdy}} \tag{20}$$

We choose the distance $z_f = 1$ μm to assure the beam has not begun to diverge; its physical size is then well adapted to the ring shaped waveguide in the fiber. Clearly the overlap integral (20) will vary with OAM mode order number. Our figure of merit is the worst case coupling loss across all modes, IL_{max}. We sweep R_c from 3 μm to 8.5 μm and w_0 from 1.5 μm to 7 μm and find IL_{max} for each case. Results are plotted in Fig. 4 for different values of m. The color bar shows the loss in dB. The same method could be used to study other figures of merit such as loss, crosstalk, mode purity, etc.

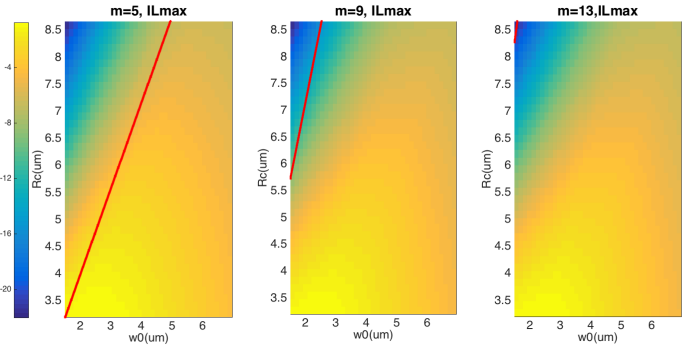

Fig. 4: Maximum coupling loss (dB) among all supported modes for three values of m

Our first observation is that IL_{max} appears insensitive to m; the color maps are virtually identical for all three plots in Fig. 4. However, we must take into account that all combinations of R_c and w_0 are physically realizable, and that the realizable regions varies greatly with m. If the beam waist is too large, there is no room to place m 2D-GCs around a circle of radius R_c. Assuming a separation of 1 μm between 2D-GCs gives

$$2\pi R_c \geq m(2w_0 + 1\ \mu\mathrm{m}) \tag{21}$$

Grating-based nano-antennas can be as small as 3 μm in length with only five grating teeth [23], thus we assume 1.5 μm as the minimum value for w_0 with sufficient efficiency. The red lines in Fig. 4 represent the boundary according to (21) for this w_0. Combinations below this line are not realizable. We can see that as the number of grating couplers grows (reading plots left to right in Fig. 4) the feasible combinations becomes less available. While larger m leads to less discretization and greater modal purity [21], it also forces us to regions of higher coupling loss.

For $m = 5$ the minimum $IL_{max} = 1.16$ dB is achieved at $R_c = 3.2$ μm, $w_0 = 1.5$ μm in the realizable region. At $m = 9$ the minimum $IL_{max} = 7.96$ dB is at $R_c = 5.86$ μm, $w_0 = 1.5$ μm. The reduction in IL_{max} is expected. While having more 2D-GCs in the ring improves phase and amplitude fidelity vis-a-vis OAM generation, it also leads to large R_c

(minimum of 5.86 μm for $w_0 = 1.5$ μm). For $m = 13$, IL_{max} grows to 18.3 dB at $R_c = 8.4$ μm, $w_0 = 1.5$ μm, making it a marginal component. Note that IL_{max} increases very quickly with R_c, and thus performance would be more vulnerable to fabrication errors in R_c.

C. Multiplexer crosstalk for target design

Given discussions in the previous section, we selected a target design with lowest IL_{max}, and in this section we examine crosstalk performance for this choice. The optimal point falls on the lowest point of the red line in the $m = 5$ plot of Fig. 4, i.e., $R_c = 3.2$ μm, $w_0 = 1.5$ μm. The crosstalk between modes i and j is defined as outputting mode i from the multiplexer and forming the ratio of the fiber-coupled power of targeted mode i to the fiber-coupled power of unintended mode j. Results are displayed in matrix form in Fig. 5 with the color map giving crosstalk in dB.

On the diagonal, the generated mode is coupled to the corresponding fiber OAM mode, giving us the coupling loss (maximum is -1.16 dB). Off-diagonal entries are the crosstalk. The highest crosstalk in Fig. 5 is -20 dB and is observed between mode pairs LH2 & RH0, RH-2 & LH0, LH-2 & RH2, and LH2 & RH-2. Note that the crosstalk between mode pairs LH-2 & RH2 and LH2 & RH-2 are due to the overlap of fiber mode profiles. That is, in these cases the multiplexer correctly generates the OAM mode, but the mode profiles in the fiber cause the crosstalk at coupling.

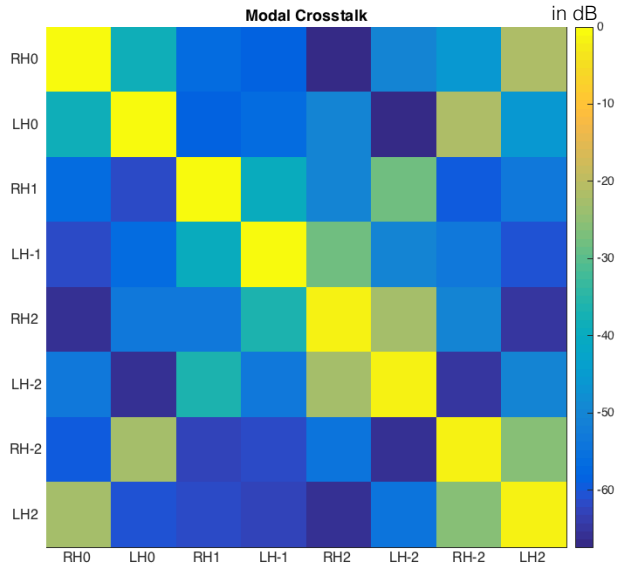

Fig. 5: Multiplexer crosstalk in dB for design with $m = 5$, $R_c = 3.2$ μm, $w_0 = 1.5$ μm

D. Tolerance analysis of loss

While we have addressed the coupling efficiency of the optical input and output in section III.B., we must also take into account losses from the star coupler. The influence of the amplitude non-uniformity in star coupler is discussed in section B of the appendix. In this section we assume uniform amplitude. For uniform amplitude, we found in the previous section the star coupler design that gives lowest IL_{max}. This design has loss from the star coupler amounting to around 7 dB; the IL_{max} itself is 1.16 dB. Taking into account coupling loss of about 3 dB at input and at output, the overall loss is less than 15 dB for this design. This estimation is pretty conservative. The loss from the star coupler could be reduced through better waveguide taper designs. 2D grating couplers with fiber-coupling loss lower than 2 dB have been demonstrated.[24]

These nominal loss values are subject to deterioration in practical systems due to misalignment, whether during fabrication or packaging/use. We examine the impact of misalignment of the chip with the OAM fiber, which will occur during packaging or during testing of the chip. Alignment deviation results in extra coupling loss and extra crosstalk. We present in Fig. 6 the influence of alignment deviation on these critical parameters. As the impact of misalignment varies with OAM mode order (topological charge), we examine each one separately.

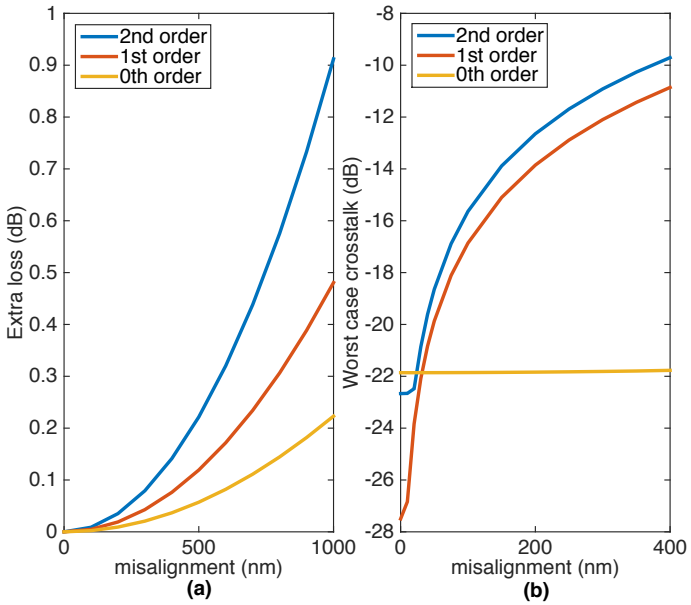

Fig. 6: The effect of misalignment for three orders of OAM modes: (a) extra loss vs. misalignment and (b) crosstalk vs. misalignment

Due to the circular symmetry of our design, the misalignment is quantified by the radial distance (i.e., distance from the origin or center of the 2D-GC ring). The second order OAM mode has the highest extra loss against misalignment, followed by the first order, then the 0^{th} order. The rate of loss increases with misalignment. For a misalignment up to 1 μm, the extra loss, Fig. 6(a), for any supported OAM mode is below 1 dB.

In Fig. 6(b), we consider the worst-case crosstalk, across a row of the modal crosstalk matrix. That is, for a first order OAM mode we consider the worst case crosstalk of that mode with the zero and second order modes, etc. In this case, the crosstalk deteriorates rapidly within the first 200 nm for the first and second order OAM modes. The zero order OAM mode (the fundamental mode) shows almost no change in

crosstalk with misalignment, even at 400 nm. This is most likely due to the zero order mode having uniform phase at every 2D-GC, while other modes have a non-uniform phase distribution across 2D-GCs. The first order OAM mode is most vulnerable. For a misalignment up to 400 nm, the crosstalk for the first and second order OAM modes are at the -10 dB level. Packaging will help in reducing misalignment and avoiding these effects.

The center deviation is a common problem in 2D grating coupler designs. The generation of circular polarization in our design relies on perfect overlapping of beams from both arms of the 2D-GC. A deviation between the centers of these arms could lead to deviations in the local polarization. For the target design where the waist of the beam is w0 =1.5 μm, we simulated a deviation of up to 1.5 μm along their own propagation axis for both arms of the 2D-GC, and in both (forward and backward) directions. A maximum of 2 dB extra loss is observed at 1.5 μm deviation, confirming that care is required in designing the 2D-GCs.

IV. Conclusion

We have presented the design and optimization methodology of a SOI based OAM generator and multiplexer that is able to generate OAM in a target circular polarization, be it right or left. The OAM generator and multiplexer demonstrated is targeting at direct OAM fiber coupling. Since no free-space optics are needed for polarization controlling or mode size conversion before coupling to OAM fiber, the loss and system complexity are definitely reduced.

The proposed structure provides a scalable multiplexing solution. Firstly, the design parameters are flexible and can be customized for different OAM fibers. Although we have focused our discussion on the transmitter side, considering the proposed device as an OAM emitter and multiplexer in our model, it should be noted that the device can also be used as an OAM demultiplexer. In addition, all the components involved in this scheme are broadband, making it WDM compatible.

Future work includes experimental demonstration and examination of performance tolerance to fabrication errors. Tuning mechanisms (e.g., using on-chip VOAs and micro-heaters) are likely needed to compensate for magnitude and phase errors due to design and fabrication imperfections. Furthermore, since all the essential components (such as the 2D-GCs, DCs, and SCs) were designed for fabrication using the standard 220-nm SOI process, the proposed multiplexer can be readily integrated with other photonic devices, such as WDM filters [25], high-speed CMOS-photonics modulators [26] and Ge photo detectors [27], on the same platform for on-chip integrated WDM-OAM transmitters and receivers for ultra-high-capacity optical transmission systems.

V. Appendix

A. Field distribution and polarization state at 2D-GC output

We simulate a single 2D-GC with 3D FDTD to 1) compare its field with a Gaussian beam and 2) observe the output polarization. The simulation model is shown in Fig. 7.

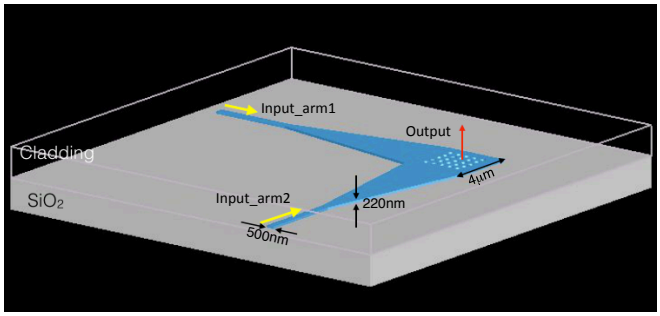

Fig. 7: 2D-GC FDTD simulation model

Two Gaussian sources are placed at the input waveguides with a 90 degree phase shift. The 500 nm wide input waveguides are broadened to 4 μm through tapers. The period in the grating region is 560 nm and the filling factor is 0.5. There are 5 periods in both direction which gives a grating region of roughly 3 μm $\times$ 3 μm; this offers the most flexibility in increasing the number of couplers in the 2D-GC ring and a good compromise in loss. We calculate numerically the electrical field $E_{2D\text{-}GC}$ for each axial distance z. We set an observation window in the simulator of 30 μm $\times$ 30 μm. The overlap integral is found between the 2D-GC field and Gaussian field along the z axis

$$\frac{\iint \mathbf{E}_G^* \cdot \mathbf{E}_{2D-GC} dxdy}{\sqrt{\iint \mathbf{E}_G^* \cdot \mathbf{E}_G dxdy \iint \mathbf{E}_{2D-GC}^* \cdot \mathbf{E}_{2D-GC} dxdy}} \tag{22}$$

The results are presented in Fig. 8.

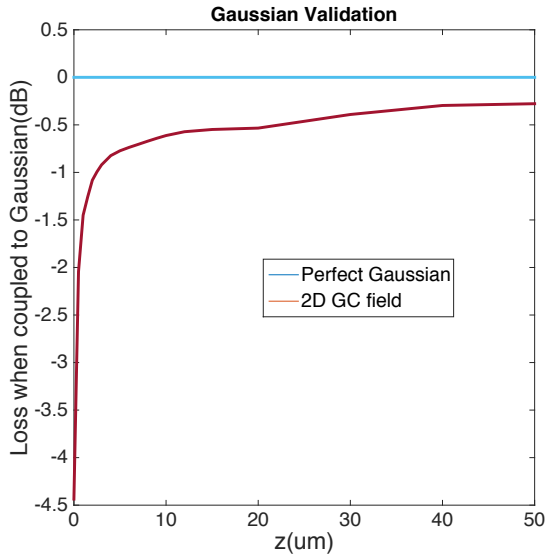

Fig. 8: Overlapping integral along z axis

A perfect Gaussian beam would give 0 dB overlap, as shown with the blue line. The red line is the case with our 2D-GC field. Due to evanescent field in the cladding, the loss when coupled to Gaussian is as high as -4.5 dB at $z = 0$ μm. As the 2D-GC beam propagates, the influence of the evanescent field decays. At $z = 1$ μm, where the coupling to OAM fiber happens, the loss is reduced to -1.5 dB. As z increases the

influence of the evanescent field diminishes, and at $z = 40$ μm, the loss is as low as -0.3 dB.

Although not presented here, we used these FDTD simulations to verify the polarization state was indeed circular. In particular, the electrical field along the z axis was observed. The polarization state changed with z displacement, tracing a circular path.

B. *Influence of amplitude non-uniformity in star coupler*

Light from the input ports of the star coupler diverges within the free propagation region. At the output ports, the amplitude varies with position. We performed FDTD simulations on the $m = 5$ case, geometry shown in Fig. 9, to assess the variation.

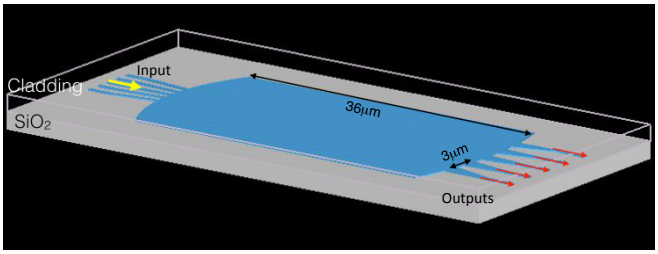

Fig. 9: Star coupler FDTD simulation model

The length of the free propagation region is chosen to be 36 μm to ensure a small footprint; the corresponding separation between the output ports at the end of the free propagation region is 3 μm. We found the 5×5 star coupler having a maximum amplitude non-uniformity of around 25%. The modal crosstalk in dB with this non-uniformity is calculated numerically. Results are presented in matrix form in Fig. 10.

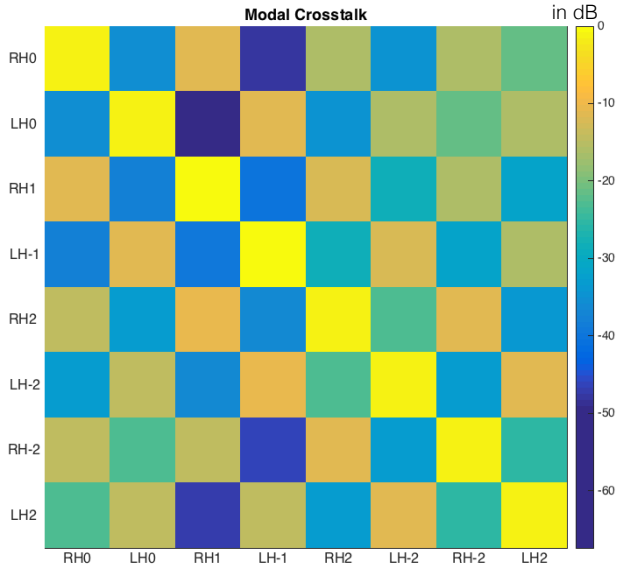

Fig. 10: Multiplexer crosstalk in dB for design with $m = 5$, $R_c = 3.2$ μm, $w_0 = 1.5$ μm taking into account non-uniform amplitude at star coupler output

The influence of the amplitude non-uniformity on coupling loss (the diagonal of the matrix) is negligible. However, the crosstalk (off diagonal) performance is much worse than that of Fig. 5, where uniform amplitude was assumed. Coupling between RH1 & LH0, LH-1 & LH0, RH2 & RH0, LH-2 & LH-1, RH-2 & RH2, and LH2 & LH-2 are on a -10 dB level.

Increasing the length of the free propagation region could potentially reduce the amplitude non-uniformity since the lateral separation could be reduced in achieving the optical path difference. However, with only 5 output ports, the amount of light that is not collected will be considerable i.e., the loss would be much higher. The trade off between the footprint, loss and amplitude non-uniformity should be better balanced in our future design.

REFERENCES

[1] C. Brunet and L. A. Rusch, "Invited paper: Optical fibers for the transmission of orbital angular momentum modes," *Optical Fiber Technology*, 2016.

[2] S. Randel, R. Ryf, A. Sierra, P. J. Winzer, A. H. Gnauck, C. A. Bolle, R.-J. Essiambre, D. W. Peckham, A. McCurdy, and R. Lingle, "6× 56-gb/s mode-division multiplexed transmission over 33-km few-mode fiber enabled by 6× 6 mimo equalization," *Optics Express*, vol. 19, no. 17, pp. 16 697–16 707, 2011.

[3] R. Ryf, S. Randel, A. H. Gnauck, C. Bolle, A. Sierra, S. Mumtaz, M. Esmaeelpour, E. C. Burrows, R.-J. Essiambre, P. J. Winzer *et al.*, "Mode-division multiplexing over 96 km of few-mode fiber using coherent 6 6 mimo processing," *Journal of Lightwave technology*, vol. 30, no. 4, pp. 521–531, 2012.

[4] A. E. Willner, H. Huang, Y. Yan, Y. Ren, N. Ahmed, G. Xie, C. Bao, L. Li, Y. Cao, Z. Zhao *et al.*, "Optical communications using orbital angular momentum beams," *Advances in Optics and Photonics*, vol. 7, no. 1, pp. 66–106, 2015.

[5] A. M. Yao and M. J. Padgett, "Orbital angular momentum: origins, behavior and applications," *Adv. Opt. Photon.*, vol. 3, no. 2, pp. 161–204, Jun 2011.

[6] N. Bozinovic, Y. Yue, Y. Ren, M. Tur, P. Kristensen, H. Huang, A. E. Willner, and S. Ramachandran, "Terabit-scale orbital angular momentum mode division multiplexing in fibers," *Science*, vol. 340, no. 6140, pp. 1545–1548, 2013.

[7] R. M. Nejad, K. Allahverdyan, P. Vaity, S. Amiralizadeh, C. Brunet, Y. Messaddeq, S. LaRochelle, and L. A. Rusch, "Mode division multiplexing using orbital angular momentum modes over 1.4-km ring core fiber," *Journal of Lightwave Technology*, vol. 34, no. 18, pp. 4252–4258, 2016.

[8] P. Vaity, C. Brunet, Y. Messaddeq, S. LaRochelle, and L. A. Rusch, "Exciting oam modes in annular-core fibers via perfect oam beams," in *Optical Communication (ECOC), 2014 European Conference on*. IEEE, 2014, pp. 1–3.

[9] X. Cai, J. Wang, M. J. Strain, B. Johnson-Morris, J. Zhu, M. Sorel, J. L. OBrien, M. G. Thompson, and S. Yu, "Integrated compact optical vortex beam emitters," *Science*, vol. 338, no. 6105, pp. 363–366, 2012.

[10] J. Sun, A. Yaacobi, M. Moresco, D. Coolbaugh, and M. R. Watts, "Chip-scale continuously tunable optical orbital angular momentum generator," *arXiv preprint arXiv:1408.3315*, 2014.

[11] B. Guan, C. Qin, R. P. Scott, N. K. Fontaine, T. Su, R. Proietti, and S. Yoo, "Polarization diversified integrated circuits for orbital angular momentum multiplexing," in *Photonics Conference (IPC), 2015*. IEEE, 2015, pp. 649–652.

[12] C. Brunet, B. Ung, L. Wang, S. LaRochelle, and L. A. Rusch, "Design of a family of ring-core fibers for oam transmission studies," *Optics express*, vol. 23, no. 8, pp. 10 553–10 563, 2015.

[13] M. K. Smit and C. Van Dam, "Phasar-based wdm-devices: Principles, design and applications," *IEEE Journal of selected topics in quantum electronics*, vol. 2, no. 2, pp. 236–250, 1996.

[14] Y. Ma, Y. Zhang, S. Yang, A. Novack, R. Ding, A. E.-J. Lim, G.-Q. Lo, T. Baehr-Jones, and M. Hochberg, "Ultralow loss single layer submicron silicon waveguide crossing for soi optical interconnect," *Optics express*, vol. 21, no. 24, pp. 29 374–29 382, 2013.

[15] W. Bogaerts, D. Taillaert, P. Dumon, D. Van Thourhout, R. Baets, and E. Pluk, "A polarization-diversity wavelength duplexer circuit in silicon-on-insulator photonic wires," *Optics express*, vol. 15, no. 4, pp. 1567–1578, 2007.

[16] F. Van Laere, W. Bogaerts, P. Dumon, G. Roelkens, D. Van Thourhout, and R. Baets, "Focusing polarization diversity grating couplers in silicon-on-insulator," *Journal of Lightwave Technology*, vol. 27, no. 5, pp. 612–618, 2009.
[17] T. S. Rappaport *et al.*, *Wireless communications: principles and practice*. Prentice Hall PTR New Jersey, 1996, vol. 2.
[18] D. Vermeulen, S. Selvaraja, P. Verheyen, G. Lepage, W. Bogaerts, P. Absil, D. Van Thourhout, and G. Roelkens, "High-efficiency fiber-to-chip grating couplers realized using an advanced cmos-compatible silicon-on-insulator platform," *Optics express*, vol. 18, no. 17, pp. 18 278–18 283, 2010.
[19] X. Chen, C. Li, and H. K. Tsang, "Two dimensional silicon waveguide chirped grating couplers for vertical optical fibers," *Optics Communications*, vol. 283, no. 10, pp. 2146–2149, 2010.
[20] M. A. Bandres and J. C. Gutiérrez-Vega, "Ince–gaussian beams," *Optics letters*, vol. 29, no. 2, pp. 144–146, 2004.
[21] Y. Chen, L. A. Rusch, and W. Shi, "Design of an integrated circular-polarized oam generator/multiplexer," in *Photonics Society Summer Topical Meeting Series (SUM), 2016 IEEE*. IEEE, 2016, pp. 205–206.
[22] C. Brunet, P. Vaity, Y. Messaddeq, S. LaRochelle, and L. A. Rusch, "Design, fabrication and validation of an oam fiber supporting 36 states," *Optics express*, vol. 22, no. 21, pp. 26 117–26 127, 2014.
[23] J. Sun, E. Timurdogan, A. Yaacobi, E. S. Hosseini, and M. R. Watts, "Large-scale nanophotonic phased array," *Nature*, vol. 493, no. 7431, pp. 195–199, 2013.
[24] Z. Nong, S. Yu, Y. N. Luo, S. Gao, and X. Cai, "Low-loss two-dimensional grating coupler on soi platform with bonded metal mirror," in *CLEO: QELS_Fundamental Science*. Optical Society of America, 2017, pp. JW2A–143.
[25] W. Shi, H. Yun, C. Lin, M. Greenberg, X. Wang, Y. Wang, S. T. Fard, J. Flueckiger, N. A. F. Jaeger, and L. Chrostowski, "Ultra-compact, flat-top demultiplexer using anti-reflection contra-directional couplers for cwdm networks on silicon," *Opt. Express*, vol. 21, no. 6, pp. 6733–6738, Mar 2013.
[26] H. Sepehrian, A. Yekani, L. A. Rusch, and W. Shi, "Cmos-photonics codesign of an integrated dac-less pam-4 silicon photonic transmitter," *IEEE Transactions on Circuits and Systems I: Regular Papers*, vol. 63, no. 12, pp. 2158–2168, Dec 2016.
[27] Y. Zhang, S. Yang, Y. Yang, M. Gould, N. Ophir, A. E.-J. Lim, G.-Q. Lo, P. Magill, K. Bergman, T. Baehr-Jones, and M. Hochberg, "A high-responsivity photodetector absent metal-germanium direct contact," *Opt. Express*, vol. 22, no. 9, pp. 11 367–11 375, May 2014.

Yuxuan Chen was born in Wuhan, China, in 1992. He received his B.S. degree in Opto-Information Science and Technology from Huazhong University of Science and Technology, Wuhan, China in 2014. He is currently working toward his Ph.D. degree at the Department of Electrical and Computer Engineering, Université Laval, Québec, QC, Canada. His research interests include photonic integrated circuit design, and simulation and characterization of space division multiplexing systems.

Leslie A. Rusch (S'91-M'94-SM'00-F'10) received the B.S.E.E. degree (with honors) from the California Institute of Technology, Pasadena, CA, USA, in 1980 and the M.A. and Ph.D. degrees in electrical engineering from Princeton University, Princeton, NJ, in 1992 and 1994, respectively. She holds a Canada Research Chair in *Communications Systems Enabling the Cloud*, is a full Professor in the ECE Department at Universit Laval, QC, Canada, where she is also a member of the Centre for Optics, Photonics, and Lasers (COPL). She has experience in defense, industrial, and academic communications research. She was a communications project engineer for the Department of Defense from 19801990. While on leave from Universit Laval, she spent two years (20012002) at Intel Labs creating and managing a group researching new wireless technologies. Prof. Rusch performs research on wireless and optical communications. Her research interests include digital signal processing for coherent detection in optical communications, spatial multiplexing using orbital angular momentum modes in fiber, radio over fiber, and OFDM for passive optical networks; and in wireless communications, optimization of the optical/wireless interface in emerging cloud based computing networks, and implantable medical sensors with high bit rate UWB telemetry. She is recipient of the IEEE Canada Fessenden Award for Telecommunications research, and the IEEE Canada J. M. Ham Award for Graduate Supervision. Prof. Rusch has published over 130 journal articles in international journals (90% IEEE/IEE) with wide readership, and contributed to over 165 conferences. Her articles have been cited over 5100 times per Google Scholar.

Wei Shi (S'07-M'12) received the Ph.D. degree in electrical and computer engineering from the University of British Columbia,Vancouver, BC, Canada, in 2012. He is currently an Assistant Professor with the Department of Electrical and Computer Engineering, Université Laval, Québec, QC, Canada. During the Ph.D. degree, he received many awards and scholarships including the BCIC Innovation Scholarship. Before joining Université Laval in 2013, he was a Researcher at McGill University, Montreal, QC, Canada, where he held an NSERC Postdoctoral Fellowship. His research interests include silicon photonics and integrated electronic- photonic systems for high-capacity optical transmissions.